Robotica (2015) volume 33, pp. 366–384. © Cambridge University Press 2014
doi:10.1017/S0263574714000241

Design and kinematic analysis of redundantly actuated parallel mechanisms for ankle rehabilitation

Congzhe Wang, Yuefa Fang*, Sheng Guo and Changchun Zhou

School of Mechanical, Electronic and Control Engineering, Beijing Jiaotong University, Beijing 100044, P.R. China

(Accepted February 2, 2014. First published online: March 3, 2014)

SUMMARY

In this paper, we present the design of two serial spherical mechanisms to substitute for a single spherical joint that is usually used to connect the platform with the base in three degrees of freedom parallel mechanisms. According to the principle derived from the conceptual design, through using the two serial spherical mechanisms as the constraint limb, several redundantly actuated parallel mechanisms are proposed for ankle rehabilitation. The proposed parallel mechanisms all can perform the rotational movements of the ankle in three directions while at the same time the mechanism center of rotations can match the ankle axes of rotations compared with other multi-degree-of-freedom devices, due to the structural characteristics of the special constraint limb and platform. Two special parallel mechanisms are selected to analyze their kinematical performances, such as workspace, dexterity, singularity, and stiffness, based on the computed Jacobian. The results show that the proposed scheme of actuator redundancy can guarantee that the redundantly actuated parallel mechanisms have no singularity, better dexterity, and stiffness within the prescribed workspace in comparison with the corresponding non-redundant parallel mechanisms. In addition, the proposed mechanisms possess certain reconfigurable capacity based on control strategies or rehabilitation modes to obtain sound performance for completing ankle rehabilitation exercise.

KEYWORDS: Ankle rehabilitation; Parallel mechanisms; Actuator redundancy; Singularity; Stiffness.

1. Introduction

The human ankle joint complex (AJC) is one of the major weight bearing structures in the body. As a result of this function and partly due to its structure, the ankle is the most commonly injured joint, particularly for basketball and soccer players. Besides, neurological impairment after stroke also can lead to the weakness of muscles around the ankle causing the inability of an individual to move their foot.[1] To regain the ability of motion, a patient has to undertake physical therapy, involving rehabilitation. Ankle rehabilitation should be done slowly and carefully, starting with non-weight bearing exercises, moving to resisted exercises, and then weight bearing activities as the ankle recovers. But traditional rehabilitation therapy is a costly labor, which requires plenty of time and patience. To reduce the physical workload and enhance the productivity of physiotherapists, rehabilitation robotics is used and just beginning to play a great role in physical therapy.

More recently, ankle rehabilitation devices (ARD) have started to be developed by making use of automatic systems to enforce or restore ankle motions specifically. These systems can be grouped into active foot orthoses[2–5] and stationary devices.[6–13] One of the successful active foot orthoses is the AAFO, an active variable-impedance orthoses that have certain clinical benefits for the treatment of drop-foot gait compared to conventional ankle-foot orthoses that patients wear while walking over ground.[2] On the contrary to active foot orthoses, the patient is always placed in the same

* Corresponding author. E-mail: yffang@bjtu.edu.cn

position without walking in a stationary system. The NUVABAT is a 2-DOF (degree of freedom) mechatronic stationary device with a virtual reality interface that can perform ankle and balance rehabilitation.[7] The prominent product of several commercial stationary devices may be the Biodex system 4,[8] which can facilitate to achieve ROM/strengthening, and perform ankle inversion/eversion and plantarflexion/dorsiflexion respectively, but the system can't realize more complex movement. To solve this problem, many researchers have been exploiting rehabilitation devices making use of parallel mechanism, characterized by its considerably complex motion and high stiffness that just match the properties of the human ankle. The "Rutgers Ankle" orthopedic rehabilitation interface, based on a 6-DOF Stewart platform that applies variable forces and virtual reality exercises on the patient's foot, can perform any complicated spatial motions.[9] But the translation of the foot segment relative to the shank segment is slight and can be neglected in rehabilitation, in other words, 3-DOF rotations may serve well to describe the ankle motions. Thus, some lower-mobility parallel mechanisms for ankle rehabilitation were introduced subsequently. Dai *et al.*[10] proposed a 3- or 4-DOF parallel mechanisms with a central strut for ankle rehabilitation and analyzed the mobility and the stiffness. Liu *et al.*[11] discussed the 3-RSS/S parallel robot with three DOFs for ankle rehabilitation. To overcome singularity inside the workspace that parallel mechanisms intrinsically possess, a special 2-DOF redundantly actuated parallel mechanism also with a central strut was developed and proved to have sound performances than the non-redundant one.[12] However, all the mentioned mechanisms[10–12] have the same problem: the mechanism axes of rotation are far offset from the ankle axes of rotation, causing unexpected movements to patients, such as translations induced by rotations, which is much worse for the patient whose shank can't move arbitrarily. To address this problem, Tsoi *et al.*[13] proposed a 3-DOF redundantly actuated parallel robot with a middle passive link that is replaced with the lower limb of the actual patient. The robot can match the nominal center of ankle rotation and avoid singularity in the workspace through adding one more limb actuation, but unexpected loads may be exerted on the patient's foot, when rehabilitation exercises start.

From the development of ARDs mentioned above, it's still a tough problem to design a 3-DOF parallel mechanism for ankle rehabilitation with a simple structure, simultaneously satisfying the condition of ensuring that the mechanism center of rotations matches the ankle axes of rotations as closely as possible while having no singularity and sound performance in workspace. Therefore, we have designed two special serial spherical mechanisms as the constraint limb to construct several new 3-DOF parallel mechanisms for addressing the issue of centers' non-coincidence. Moreover, a new arrangement of actuator redundancy is proposed to eliminate singularity and improve kinematic performances within the workspace. As such, the proposed parallel mechanisms possess certain reconfigurable capacity based on control strategies or rehabilitation modes to obtain sound performance for completing ankle rehabilitation exercises.

The presentation of this work is structured as follows. In Section 2, the anatomy and kinematics of ankle are introduced and then the conceptual design is detailed. The forward, inverse kinematics and Jacobian analysis are studied In Section 3. Kinematic performances such as workspace volume, dexterity, singularity, and stiffness are studied In Section 4. Finally, conclusion and further developments of this work are given in Section 5.

2. Design Specification and Conceptual Design

2.1. Design specification

As shown in Fig. 1,[14] the human ankle joint complex (AJC) consists of two separate subjoints: the true ankle joint and the subtalar joint.[15] Dettwyler *et al.*[16] concluded that motion of the foot-shank complex is the result of a simultaneous motion at the talocrural and subtalar joints, where neither of these two joints has a fixed axis and the subtalar axis especially shows a greater variability. Hence, angular displacements in the two ankle joints produce rotations of the foot in the sagittal, frontal, and transverse planes and the rotations can be defined as plantar/dorsiflexion, inversion/eversion, and adduction/abduction (also called internal/external rotation), as illustrated in Fig. 2. The more complicated motion is adduction/abduction achieved through a combination of the motions of the two subjoints, as well as rotation of the tibia and fibula.[15] Thanks to previous work, the estimated

https://doi.org/10.1017/S0263574714000241 Published online by Cambridge University Press

Fig. 1. Ankle joint complex.[14]

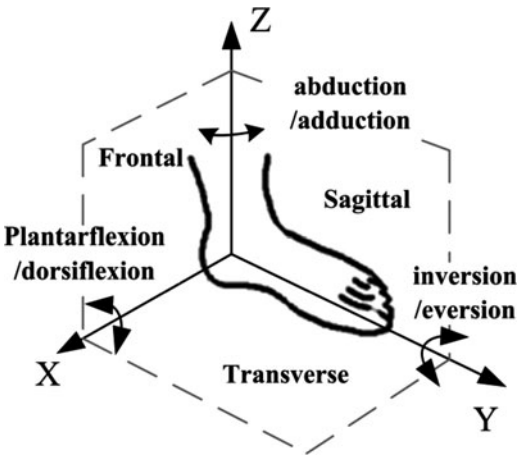

Fig. 2. Definitions on the ankle motion.

Table I. Range of motion of the AJC[13].

Type of motion	Max. allowable motion
Dorsiflexion	$20.3^\circ - 29.8^\circ$
Plantarflexion	$37.6^\circ - 45.8^\circ$
Inversion	$14.5^\circ - 22.0^\circ$
Eversion	$10.0^\circ - 17.0^\circ$
Abduction	$15.4^\circ - 25.9^\circ$
Adduction	$22.0^\circ - 36.0^\circ$

range of motion (ROM) of the AJC in each direction is given in Table I.[13] It is worthy of noting that the ROM can vary greatly among different persons.

Although some researches indicated that the first two motions are the dominant actions in proprioceptive training and ankle rehabilitation,[12] exercises that involve the abduction or adduction of the foot, such as drawing the alphabet letters, are still included in rehabilitation protocols. After all for the ankle rehabilitation, the joints, tendons, and muscles as a whole unit are to be exercised throughout of all the range of motion. Moreover, 3-DOF rotations can finish more complex trajectories that are helpful for rehabilitation exercise. In a word, the third rotation is necessary for ankle rehabilitation,

https://doi.org/10.1017/S0263574714000241 Published online by Cambridge University Press

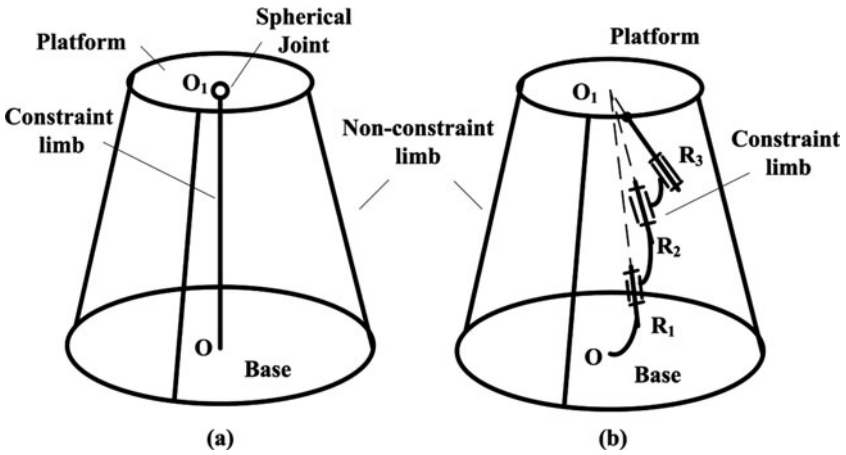

Fig. 3. Constraint limb with a single spherical joint (a), or a serial spherical mechanism (b).

so our objective is to design an ARD with 3-DOF rotational movements that satisfies the motion requirements and has high torque output.

2.2. Conceptual design

It is obvious that any serial spherical mechanism can be one possible alternative to actualizing 3-DOF rotations, such as gimbal mechanisms. One characteristic of serial mechanisms is related to the fact that the actuator of the first joint must bear the weight of the others. On the contrary, all the actuators in parallel mechanisms are mounted on the ground, which brings one advantage that parallel mechanisms provide larger forces than serial mechanisms with the same sized actuators. While considering the design of an ankle rehabilitation device, due to the rotations allowable at the AJC involved with large moments, parallel mechanisms are more competent than serial mechanisms particularly when performing 3-DOF rotations. However, the parallel mechanism has its own drawbacks, such as small available workspace, singularity caused by complex configurations or constraints, which restrain its practical application in industry and real life. Except for the 6-DOF Gough-type parallel manipulators extensively used in industry, there are just several types of lower-mobility parallel manipulators succeeding in application, such as Delta,[17] H4,[18] Tricept,[19] Agile eye.[20] Therein, the Agile eye is a spherical manipulator that can actualize 3-DOF rotational movements, but its geometrical constraints are so complex that it couldn't be fully satisfied if forces and moments acted on the platform are large. Interestingly, the Tricept manipulator is different from the others in terms of type design. It is composed of a platform linked to the base (ground) by three identical non-constraint limbs (UPS limb) and the constraint UP limb (the letter P represents a prismatic joint, U a universal joint, and S a spherical joint). The constraint limb determines the degrees of freedom and the motion characteristic of the Tricept; adding one actuator into each non-constraint limb can actuate the mechanism and the number of non-constraint limbs is commonly equal to the DOFs. This type design at some extent incorporates the merits of both parallel mechanisms and serial mechanisms. According to the type design theory, a 3-DOF spherical parallel mechanism can be easily deduced, just substituting the UP limb with a spherical limb, such as reference.[10] In fact, the general method is to use a single spherical joint linking the platform with the base, but it raise the problem as mentioned above: the mechanism axes of rotation are far offset from the ankle axes of rotation, causing unexpected movements to patients. On the other hand, the serial spherical mechanism has its own separate axis that can be conveniently rearranged, so why not substitute the single spherical joint with the serial spherical mechanism? Then Fig. 3 depicts the two different structures, where the letter R represents a revolute joint. Figure 3(a) displays the usual structural arrangement with a single spherical joint; Fig. 3(b) shows that the constraint limb is made up of a serial spherical mechanism, three axes of which may be oriented in any arbitrary direction, but intersect at the center O_1. Certainly, one available alternative is the case of the three axes that are, respectively, parallel to the vertical, the sagittal, and the frontal ones. After considering kinematic and dynamic performance, we proposed two kinds of serial spherical mechanisms, or called equivalent spherical joint, with symmetrical structure as shown

https://doi.org/10.1017/S0263574714000241 Published online by Cambridge University Press

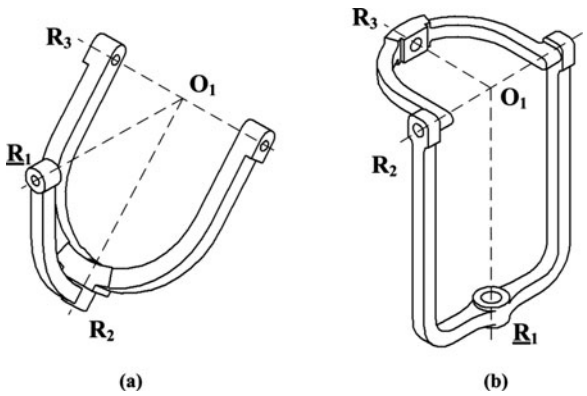

Fig. 4. Two serial spherical mechanisms: the axes of R_1 and R_2 are not orthogonal (a), and orthogonal (b).

in Fig. 4, where the axes of R_2 and R_3 are orthogonal for the two equivalent spherical joints and the only difference lies that the axes of R_1 and R_2 are not orthogonal for the first shown in Fig. 4(a), but orthogonal for the second shown in Fig. 4(b).

Subsequently, we still do not address the problem that singularity lies in the workspace of parallel mechanisms. One possible choice is to add one more limb, as the research[13] did. If so, there will be four active non-constraint limbs for the mechanism depicted in Fig. 3(b). Then every single movement needs to be fulfilled by precise cooperation of the four limbs, which is not energy-efficient and possibly increases interference. In order to make use of the kinematical feature of the serial spherical mechanism, the redundant actuator will be added on the revolute joint linked to the base (the $\underline{R}_1$ joint is actuated and signified by an underline as shown in Fig. 4) instead of adding one more limb. The non-constraint limb has many choices, such as UPS limb, RUS limb, or even cable driven limb. Here the UPS limb is selected for its fitness to utilize all the two spherical mechanisms, so the novel 3-U$\underline{P}$S/$\underline{R}$RR redundantly actuated parallel mechanism is what we desire. Then the following sections will discuss the effectiveness of this actuator redundancy arrangement.

The CAD models of the 3-U$\underline{P}$S/$\underline{R}$RR redundant parallel robot for ankle rehabilitation are developed as shown in Fig. 5. The first spherical mechanism is applied to the two mechanisms as illustrated in Figs. 5(a) and 5(b), denoted as ARDS1-R and ARDS1-R2 respectively, but the directions of the axes of R_1 joint are different; the second spherical mechanism is applied to the third mechanism shown in Figs. 5(c) and 5(d), denoted as ARDS2-R. To enlarge the motion angle, the spherical joint is redesigned, consisting of three single revolute joints. Besides, the platform is made up of two parts: the lower and upper platforms; the position of the upper platform relative to the lower one can be adjusted by a screw mechanism; meanwhile, the platform shapes the profile of the human being's foot. Owing to the novel mechanical design of the serial spherical mechanism and platform, the mechanism center of rotations can easily match the ankle axes of rotations. Before starting rehabilitation exercise, as shown in Fig. 5(d), patient would better align his or her malleolus with the axis of R_2 (or R_3 for the ARDS1-R and ARDS1-R2), and adjust the distance between the bottom of foot and the axis of R_2 (or R_3) through altering the position of the upper platform. By virtual of these arrangements, the proposed mechanisms can provide good flexibility for different patients to ensure the coincidence of rotational centers while at same time possesses sound performances. Particularly, when the redundant actuator of the R_1 joint is self-locked, the ARDS2-R manipulator depicted in Fig. 5(c) becomes a 3-U$\underline{P}$S/U redundantly actuated parallel mechanism with two DOFs; in other words, this robotic system can be reconfigured into either a 2-DOF rehabilitation device or a 3-DOF one just depending on rehabilitation exercise modes, all which enhances the flexibility of the system. Although the ARDS1-R and ARDS1-R2 manipulators have distinct arrangements, they have similar kinematical performances. Hence, the two mechanisms, ARDS1-R and ARDS2-R, and their own non-redundantly actuated mechanisms (denoted as ARDS1-N and ARDS2-N respectively, that is, there are no actuators on the R_1 joints) are mainly discussed in the following sections.

https://doi.org/10.1017/S0263574714000241 Published online by Cambridge University Press

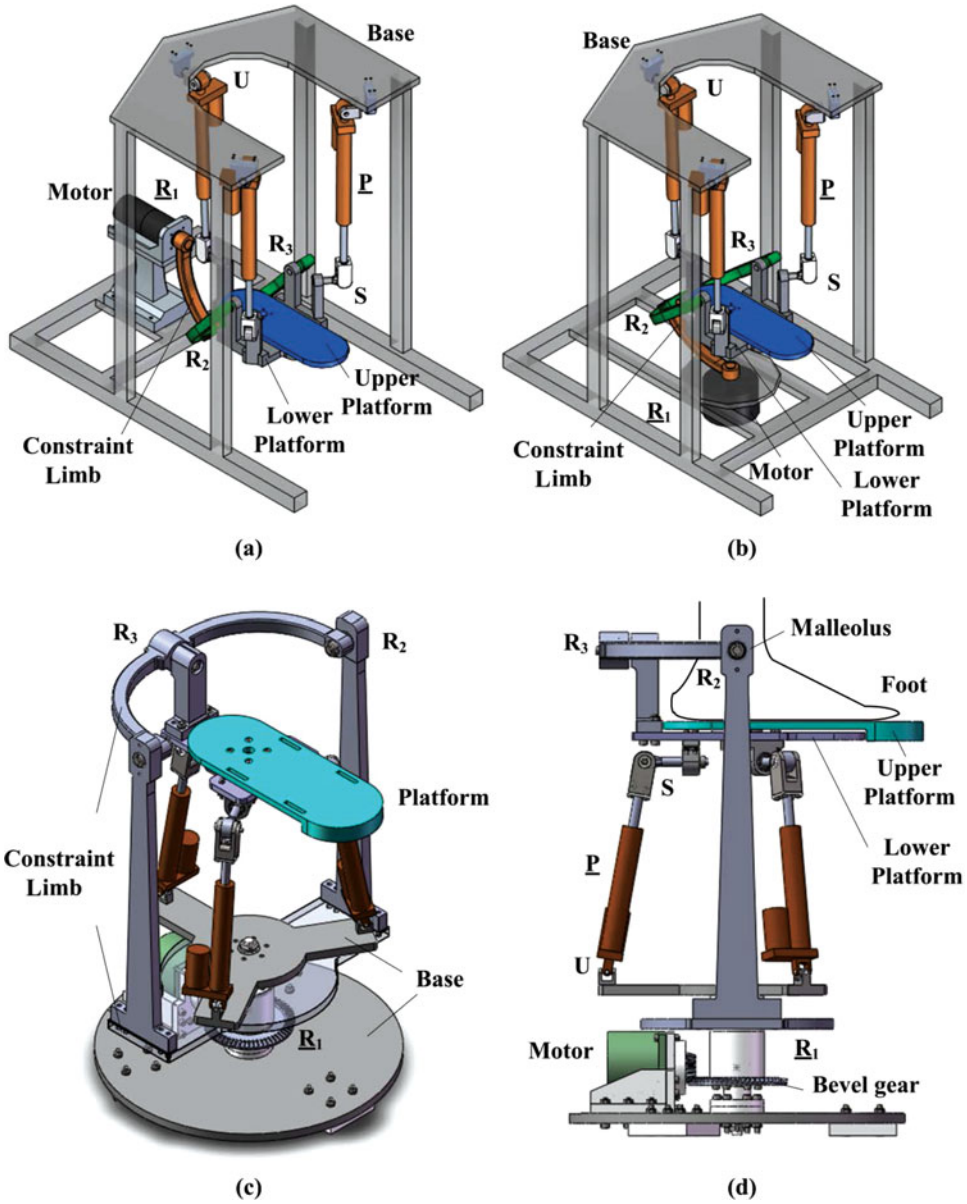

Fig. 5. CAD models of the redundantly actuated parallel mechanisms: ARDS1-R (a); ARDS1-R2 (b); ARDS2-R (c); front view of the ARDS2-R (d).

3. Kinematics Analysis

Figure 6 describes the geometrical models of the ARDS1-R and ARDS2-R redundant robots. The reference frames $X_bY_bZ_bO_b$ and $X_pY_pZ_pO_p$ attach at the base and the moving platform respectively, and locate at the center point of the machine rotations, convenient for describing the orientation of the AJC. The parameters used in kinematics are defined as follows:

$$d_1 = \left\| \overrightarrow{O_1B_i} \right\|, \quad d_2 = \left\| \overrightarrow{OA_i} \right\|, \quad l_1 = \left\| \overrightarrow{O_1O_b} \right\|, \quad l_2 = \left\| \overrightarrow{OO_b} \right\|,$$

where $A_i (i = 1, 2, 3)$ are fixed endpoints of the prismatic actuators and uniformly distributed on the base; B_i are moving endpoints of the prismatic actuators and also uniformly distributed on the lower platform; **u**, **v** and **w** are unitary vectors respectively collinear to the axes of the constraint limb; the angle between the vector **u** and **v** is determined by the geometrical constraint, defined as φ.

https://doi.org/10.1017/S0263574714000241 Published online by Cambridge University Press

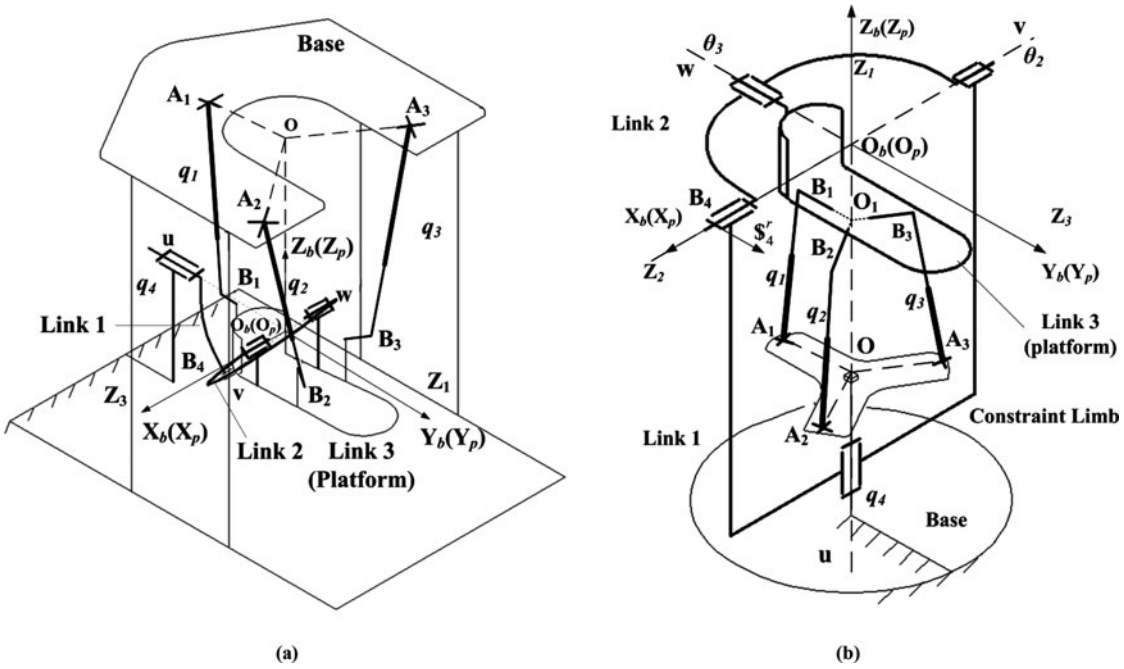

Fig. 6. Geometrical models of the ARDS1-R (a) and ARDS2-R (b).

The lengths of the three prismatic actuators are denoted as q_1, q_2, q_3; the angle around the vector **u** is denoted as q_4.

There are several ways for expressing the orientation of a moving body, such as direction cosine matrix, RPY method, Euler angles. Euler angles have many categories. Due to the characteristics of the equivalent spherical joint, the ZYX and ZXY types are respectively selected for the ARDS1-R and ARDS2-R. Here α denotes the angle of the rotation around X axis; β the angle around Y axis; γ the angle around Z axis. Once the angles are given, the orientation or rotation matrix ${}^b\mathbf{R}_p$ of the moving platform (body p) with respect to the fixed base (body b) can be easily represented as follows:

$$ {}^b\mathbf{R}_p = \mathbf{R}_z(\gamma)\mathbf{R}_y(\beta)\mathbf{R}_x(\alpha), \text{ for the ARDS1-R,} \tag{1} $$

$$ {}^b\mathbf{R}_p = \mathbf{R}_z(\gamma)\mathbf{R}_x(\beta)\mathbf{R}_y(\alpha), \text{ for the ARDS2-R.} \tag{2} $$

3.1. Forward kinematics

Forward kinematics is a tough problem for parallel mechanism, there is no exception in this study. Usually the possible orientations of the moving platform should be computed by a given set of actuators displacements, but here other ways can be selected. Thanks to the design of the equivalent spherical joint, through adding position sensors (such as optical encoders) to the joints of the constraint chain, the orientation of the platform can be calculated.

As illustrated in Fig. 4, the equivalent spherical joint is a 3-DOF chain, so its posture can be completely described by three joint variables, denoted as θ_1, θ_2 and θ_3. Applying the Denavit-Hartenberg (D-H) convention, the transformation from the moving platform to the fixed base can be written as

$$ {}^b\mathbf{T}_p = {}^b\mathbf{T}_1(\theta_1){}^1\mathbf{T}_2(\theta_2){}^2\mathbf{T}_3(\theta_3){}^3\mathbf{T}_p, \tag{3} $$

where ${}^i\mathbf{T}_j$ denotes the 4×4 D-H transformation matrix. As shown in Fig. 6, the first link frame is attached to the first moving link with the z_1 axis collinear to the vector **u**; the second link frame is attached to the second moving link with the z_2 axis collinear to the vector **v**; the third link frame is attached to the moving platform with the z_3 axis collinear to the vector **w**; ${}^3\mathbf{T}_p$ signifies the transformation from the moving frame p to the third link frame.

https://doi.org/10.1017/S0263574714000241 Published online by Cambridge University Press

Table II. D-H parameters of the constraint limb of the ARDS1-R.

Link	α_i	a_i	θ_i	d_i
Base (b)	0	0	0	0
1	-90°	0	θ_1	0
2	φ	0	θ_2	0
3	90°	0	θ_3	0
Platform (p)	-90°	0	-90°	0

Table III. D-H parameters of the constraint limb of the ARDS2-R.

Link	α_i	a_i	θ_i	d_i
Base (b)	0	0	0	0
1	0	0	θ_1	0
2	90°	0	θ_2	0
3	90°	0	θ_3	0
Platform (p)	90°	0	0	0

Equating (1) or (2) to (3) produces a loop-closure equation as follows:

$$ {}^{b}\mathbf{T}_1(\theta_1)\,{}^{1}\mathbf{T}_2(\theta_2)\,{}^{2}\mathbf{T}_3(\theta_3)\,{}^{3}\mathbf{T}_p = \begin{bmatrix} {}^{b}\mathbf{R}_p & \mathbf{0} \\ \mathbf{0} & 1 \end{bmatrix}. \tag{4} $$

Substituting the D-H parameters given in Tables II or III, and the joint angle values measured by sensors into the transformation matrixes and the resulting expression into the Eq. (4) can obtain the orientation matrix ${}^{b}\mathbf{R}_p$.

3.2. Inverse kinematics

The inverse kinematics here can be stated as follows: given the orientation (α, β, γ) of the moving platform, compute the displacements (q_1, q_2, q_3, q_4) of the actuators.

The coordinates of the points $\mathbf{B}_i (i = 1, 2, 3)$ attached at the moving platform, expressed in the reference frame $\mathrm{X}_b\mathrm{Y}_b\mathrm{Z}_b\mathrm{O}_b$ and the frame $\mathrm{X}_p\mathrm{Y}_p\mathrm{Z}_p\mathrm{O}_p$, respectively, can be represented as ${}^{b}\mathbf{b}_i$ and ${}^{p}\boldsymbol{b}_i$, and ${}^{b}\boldsymbol{b}_i$ can be computed by the equation as follows:

$$ {}^{b}\mathbf{b}_i = {}^{b}\mathbf{R}_p\,{}^{p}\mathbf{b}_i, \quad i = 1, 2, 3. \tag{5} $$

Due to the geometrical constraints, the following equality can be simply written:

$$ q_i^2 = \left({}^{b}\mathbf{a}_i - {}^{b}\mathbf{b}_i\right)^{\tau}\left({}^{b}\mathbf{a}_i - {}^{b}\mathbf{b}_i\right), \quad i = 1, 2, 3, \tag{6} $$

where ${}^{b}\boldsymbol{a}_i$ are the coordinates of the points $\boldsymbol{A}_i$ attached at the base and expressed in the reference frame $\mathrm{X}_b\mathrm{Y}_b\mathrm{Z}_b\mathrm{O}_b$.

Meanwhile, the angle between the vector $\mathbf{v}$ and $\mathbf{w}$ always stays a constant value, 90°, no matter how the orientation of the platform changes. Therefore, the following equality can be simply written:

$$ \left(\mathbf{R}_u\left(q_4\right)\mathbf{v}\right)^T\,{}^{b}\mathbf{R}_p\mathbf{w} = 0, \tag{7} $$

where $\boldsymbol{R}_u(q_4)$ a rotation matrix signifies rotating around $\mathbf{u}$ axis up to the angle of q_4, here $q_4 = \theta_1$. This relationship leads to

$$ M\sin q_4 + N\cos q_4 = T, \tag{8} $$

https://doi.org/10.1017/S0263574714000241 Published online by Cambridge University Press

where

$$M = \sin\varphi \sin\beta,$$
$$N = \sin\varphi \cos\beta \cos\gamma,$$
$$T = \cos\varphi \cos\beta \sin\gamma,$$

1) The ARDS1-R manipulator: Resorting to the new variable t = tan $(q_4/2)$ results in

$$q_4 = 2\tan^{-1}\left(\frac{-b + \sqrt{b^2 - 4ac}}{2a}\right), \tag{9}$$

where

$$a = T + N,$$
$$b = -2M,$$
$$c = T - N.$$

2) The ARDS2-R manipulator: Simplifying Eq. (9) results in

$$q_4 = \gamma \tag{10}$$

3.3. Jacobian matrix

The Jacobian matrix is to establish the relations between, on one side, the angular velocities of the platform referred to the world frame and which are grouped in the vector $\boldsymbol{w} = [w_x, w_y, w_z]^T$ and, on the other side, the active joint velocities grouped in the vector $\dot{\mathbf{q}} = [\dot{q}_1, \dot{q}_2, \dot{q}_3, \dot{q}_4]^T$. The relationship also can be represented as follows

$$\mathbf{J}_x \mathbf{w} = \mathbf{J}_q \dot{\mathbf{q}}. \tag{11}$$

According to the study of J. Gallardo-Alvarado *et al.*,[21] it's efficient for solving the problem to make use of screws and reciprocal wrenches. Let $\boldsymbol{V} = [\boldsymbol{w}^T; \boldsymbol{v}^T]^T = [\boldsymbol{w}^T; \mathbf{0}]^T$ be the instantaneous twist of the platform; where $\mathbf{v}$ is the linear velocity of a point (always coincident with the origin O_b of the base frame) fixed at the platform, and equal to $\mathbf{0}$. The twist also can be expressed through any of the four limbs as a linear combination of the joint velocity rate w as follows:

$$\mathbf{V} = \sum_{j=1}^{m_i} {}^j w_i \, {}^j\$_i, \quad i = 1, \ldots, 4, \tag{12}$$

where m_i is the number of joints of the ith limb; ${}^j\$_i$ denotes a unite screw associated with the jth joint of the ith limb; ${}^1 w_i = \dot{q}_i$ is the joint velocity rate of the active joint of ith limb.

In order to eliminate the velocities of passive joints, the concept of reciprocal wrenches will be used. With the actuators locked, a constraint wrench $\$_i^r$ being reciprocal to all the passive joint screws of each limb can be found. For limb 1, 2, 3, the constraint wrench passes through U joint and S joint; for limb 4, the wrench is parallel to the vector $\mathbf{w}$ and intersects with the vector $\mathbf{v}$. Applying the Klein form, $\{{}^*; {}^*\}$,[21] to both sides of Eq. (11) leads to the following four expressions

$$\begin{aligned}
\left\{\$_1^r; \mathbf{V}\right\} &= \dot{q}_1, \\
\left\{\$_2^r; \mathbf{V}\right\} &= \dot{q}_2, \\
\left\{\$_3^r; \mathbf{V}\right\} &= \dot{q}_3, \\
\left\{\$_4^r; \mathbf{V}\right\} &= \dot{q}_4 \cdot \left\{\$_4^r; {}^1\$_4\right\}.
\end{aligned} \tag{13}$$

https://doi.org/10.1017/S0263574714000241 Published online by Cambridge University Press

Table IV. Architectural parameters of the ARDS1-R.

Parameter	Value
φ	50 deg
d_1	0.120 m
d_2	0.130 m
l_1	0.0 m
l_2	0.335 m

Table V. Architectural parameters of the ARDS2-R.

Parameter	Value
d_1	0.120 m
d_2	0.130 m
l_1	0.110 m
l_2	0.290 m

Casting the four equations above in a matrix-vector form and Simplifying leads to

$$\begin{bmatrix} \left({}^b\mathbf{b}_1 \times \mathbf{s}_1^r\right)^T \\ \left({}^b\mathbf{b}_2 \times \mathbf{s}_2^r\right)^T \\ \left({}^b\mathbf{b}_3 \times \mathbf{s}_3^r\right)^T \\ \left({}^b\mathbf{b}_4 \times \mathbf{s}_4^r\right)^T \end{bmatrix} \mathbf{w} = \begin{bmatrix} 1 & 0 & 0 & 0 \\ 0 & 1 & 0 & 0 \\ 0 & 0 & 1 & 0 \\ 0 & 0 & 0 & \left({}^b\mathbf{b}_4 \times \mathbf{s}_4^r\right)^\tau \ \mathbf{s}_4^1 \end{bmatrix} \begin{bmatrix} \dot{q}_1 \\ \dot{q}_2 \\ \dot{q}_3 \\ \dot{q}_4 \end{bmatrix}, \tag{14}$$

where ${}^b\boldsymbol{b}_4$ is the position vector of the point $\boldsymbol{B}_4$, a point of the axis collinear to the vector $\mathbf{v}$; $\mathbf{s}_i^r$ is the unitary direction vector of the wrench $\$_i^r$; ${}^1\boldsymbol{s}_4$ is the unitary direction vector of the screw ${}^1\$_4$.

Therefore, provided $\boldsymbol{J}_q$ is invertible, the following equation can be written

$$\mathbf{J}\mathbf{w} = \dot{\mathbf{q}}, \tag{15}$$

where

$$\mathbf{J} = \mathbf{J}_q^{-1}\mathbf{J}_x.$$

4. Kinematic Performance Analysis

4.1. Workspace analysis

Inverse kinematical model has been used to determine the displacements of the actuators required to achieve the desired orientation of the platform. Once one of the displacement values exceeds the predetermined limit, the set pose is unreachable and excluded. The architectural parameters of the ARDS1-R and ARDS2-R manipulators are presented in Tables IV and V, where the two manipulators have the same values of d_1 and d_2 that mainly determine kinematical performance, and different values of l_1 and l_2, due to distinct structures. The prismatic actuator's stroke is constrained to 170 mm; the angle between $\mathrm{B}_i\mathrm{O}_1$ and $\mathrm{B}_i\mathrm{A}_i$ should be more than 40 degrees. Moreover, the constraint limb of the ARDS1-R also restricts the movement of the platform. It is obvious that the chain arrives at boundaries if all the three axes are coplanar, that is, the chain is singular and the value of the angle θ_2 is

$$\sin\theta_2 = \frac{\cos\beta\sin\gamma}{-\sin\varphi}. \tag{16}$$

https://doi.org/10.1017/S0263574714000241 Published online by Cambridge University Press

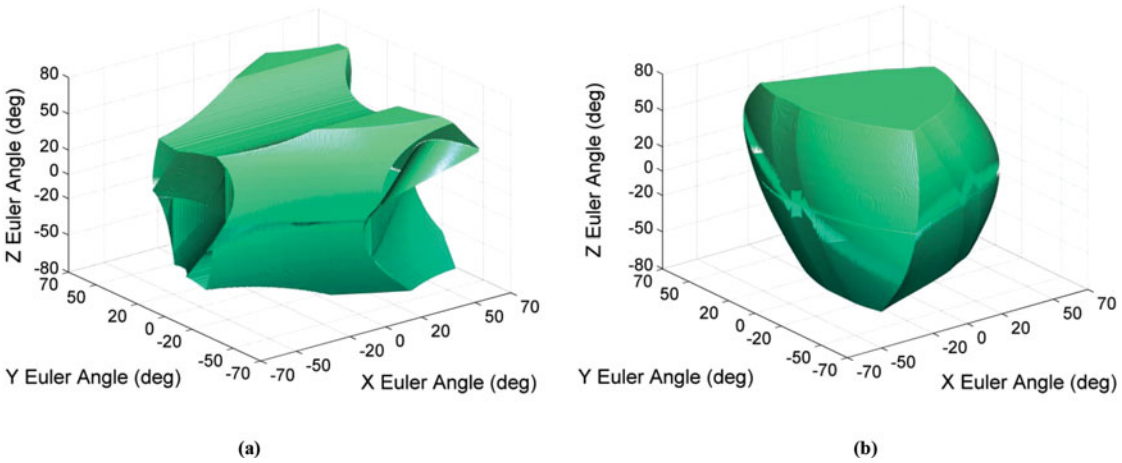

Fig. 7. The available workspaces of the ARDS1-R (a) and ARDS2-R (b).

Table VI. Workspace limits of the ARDS1-R.

Direction of motion	Angle limits
Dorsiflexion	43 deg
Plantarflexion	48 deg
Inversion/Eversion	45 deg
Abduction / Adduction	50 deg

Table VII. Workspace limits of the ARDS2-R.

Direction of motion	Angle limits
Dorsiflexion	60 deg
Plantarflexion	46 deg
Inversion/Eversion	48 deg
Abduction / Adduction	>60 deg

In view of the above equality, it can be seen that the angle θ_2 has nothing to do with the Euler angle α. When the angles β and γ meet the condition $|\sin\theta_2| \geq 1$, it means the limb lies at the boundary, so the corresponding pose should be deserted. Therefore, through discretizing the potential region for platform orientations and searching for those poses that satisfy the conditions mentioned above, the workspaces of the ARDS1-R and ARDS2-R are numerically determined and depicted in Figs. 7(a) and 7(b) separately. In fact, the non-redundant ARDS1-N and ARDS2-N respectively have the same workspace as that their own redundant type has. Owing to the restriction of the constraint limb, there is a concave surface on the top of the workspace as illustrated in Fig. 7(a), which is different from the workspace shown in Fig. 7(b). Although, the constraint limb restricts the workspace of the ARDS2-R too, but it always occurs at the workspace boundary. By analyzing various 'slice' of the workspace, the maximum achievable displacement in each direction are given in Tables VI and VII. In comparison with the statistics data of Table I, it is suggested that the devices meets the requirements of the ankle ROM. At the same time, in application, to have proper condition number and stiffness, the workspace is limited to $\pm 50^\circ$ at X Euler angle (plantar/dorsiflexion), $\pm 30^\circ$ at Y Euler angle (inversion/eversion), $\pm 40^\circ$ at Z Euler angle (adduction/abduction), and thus the following discussions are confined to the prescribed workspace.

4.2. Dexterity analysis

The condition number is often used to evaluate a mechanism's dexterity. According,[22] the condition number can be regarded as an error amplification factor, reflecting how a relative error in $\mathbf{q}$ gets multiplied and leads to a relative error in $\mathbf{x}$ (here $\mathbf{x} = \mathbf{w}$). Though here the Jacobian Matrix $\mathbf{J}$ is not a

https://doi.org/10.1017/S0263574714000241 Published online by Cambridge University Press

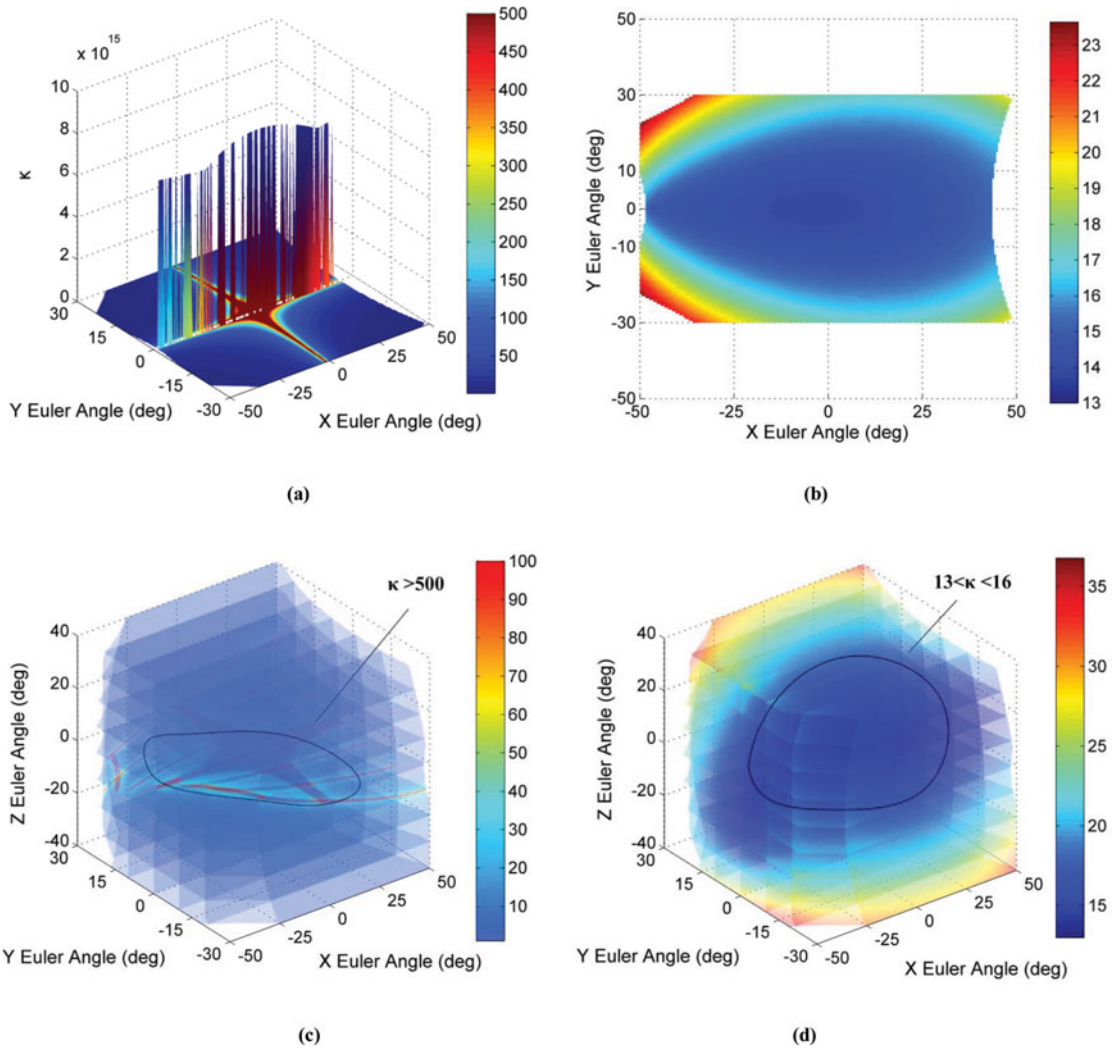

Fig. 8. The distribution of dexterity for the ARDS1-N (a) and ARDS1-R (b) in the plane of $\gamma = 0°$; the ARDS1-N (c) and ARDS1-R (d) within the whole prescribed workspace.

square matrix, its singular value σ_i still can be calculated as

$$\sigma_i = \sqrt{\lambda_i(\mathbf{J}^T\mathbf{J})}, \tag{17}$$

where λ_i is the eigenvalue of the matrix $\mathbf{J}^T\mathbf{J}$. Then the condition number κ can be given as follows:

$$1 \leq \kappa = \frac{\sigma_{\max}}{\sigma_{\min}} \leq \infty, \tag{18}$$

where $\sigma_{\max}$ and $\sigma_{\min}$ are the maximum and minimum singular values of the matrix $\mathbf{J}$, respectively.

One objective of mechanism design is to obtain reasonable values of the condition number for sound dexterity. When the condition number is equal to 1, the dexterity of the mechanism is the best and the mechanism is isotropic; conversely, if the condition number tends to infinity, the mechanism is close to singularity. Hence, the closer to 1 the condition number is, the better the dexterity of the mechanism is.[23] Figure 8 and 9 respectively illustrate the distributions of dexterity of the two redundant manipulators and their own non-redundant types. It can be observed that the condition numbers of the ARDS1-N and ARDS2-N have sudden peak values much greater than 500 in the plane of $\gamma = 0$ deg as shown in Figs. 8(a) and 9(a), which indicates that the mechanisms are nearly singular at these poses; on the contrary, the ARDS1-R and ARDS2-R have better values between 5 and 25 as shown in

https://doi.org/10.1017/S0263574714000241 Published online by Cambridge University Press

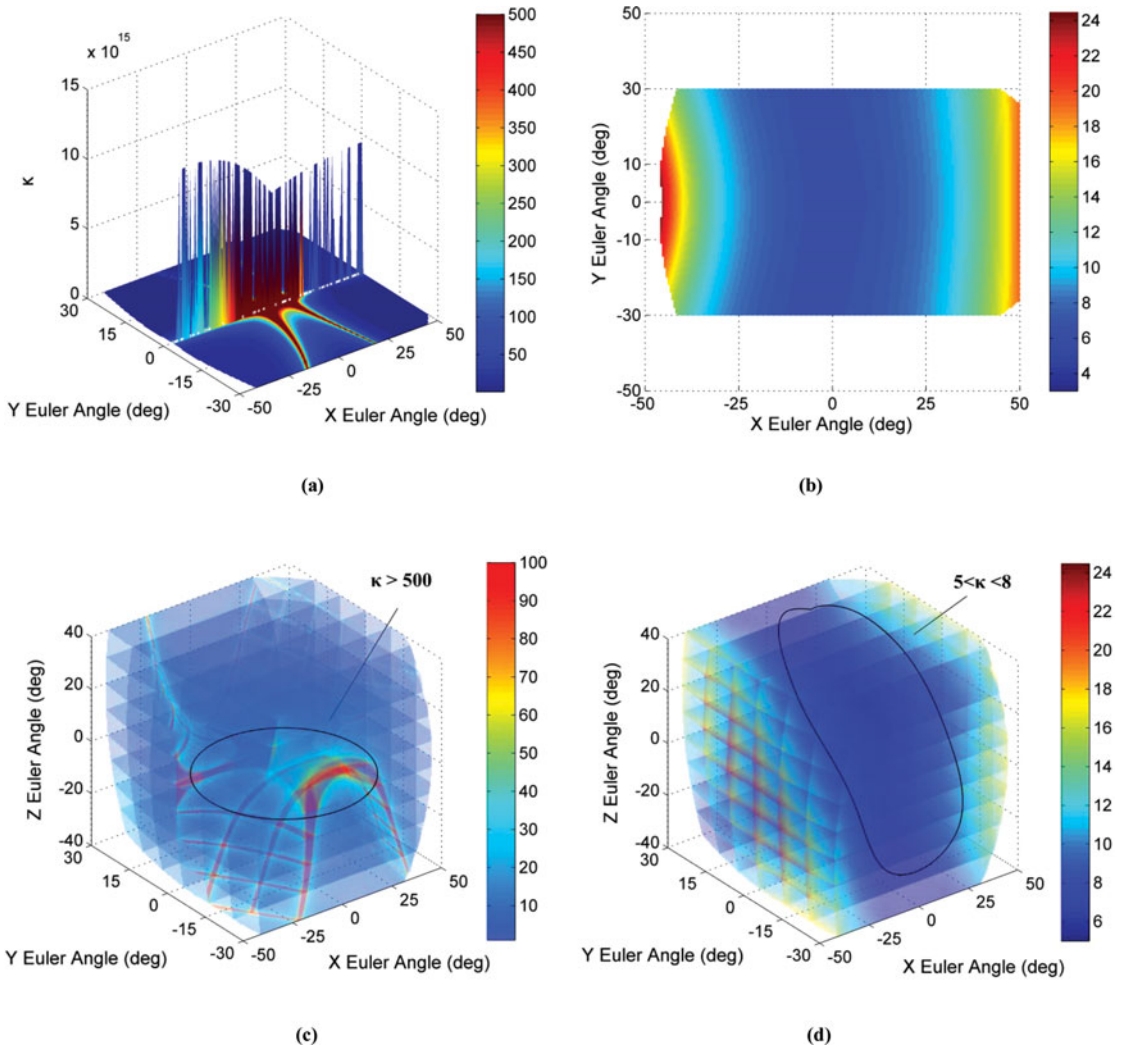

Fig. 9. The distribution of dexterity for the ARDS2-N (a) and ARDS2-R (b) in the plane of $\gamma = 0°$; the ARDS2-N (c) and ARDS2-R (d) within the whole prescribed workspace.

Figs. 8(b) and 9(b). To reveal a considerable comprehensive distribution of the condition number within the whole prescribed workspace, computing results of the four mechanisms (ARDS1-N, ARDS1-R, ARDS2-N and ARDS2-R) in three-dimensional space are respectively presented in Figs. 8(c), 8(d), 9(c) and 9(d). The results reveal that the ARDS1-N and ARDS2-N both have bad dexterity inside the middle workspace with the condition numbers greater than 500 and fine dexterity at other poses with the condition numbers smaller than 10, which is not acceptable for ankle exercises that mainly operate in the center part of the workspace; the situations of the ARDS1-R and ARDS2-R are inverse: the highest values of the condition number, more than 20 and less than 36, just occur at the boundary of the workspace and the lower values appears in the core zone, which guarantees the mechanisms have good dexterity values in the middle of the workspace. Furthermore, the condition numbers of the ARDS1-R are more than two times as large as ones of the ARDS2-R that are between 5 and 8 in the middle workspace, so theARDS2-R has better dexterity than the ARDS1-R. All the results also suggest that the condition number of redundantly actuated manipulators varies smoothly in its vicinity, has no sudden peak values and lies within a reasonable limit in the entire workspace. In addition, this analysis shows that actuator redundancy does not ensure the dexterity index of the redundant manipulator to be always superior to the non-redundant one at every pose, but indeed enhance the minimum of dexterity index, especially ones near singularity loci.

https://doi.org/10.1017/S0263574714000241 Published online by Cambridge University Press

4.3. Singularity analysis

Subsequently, the condition number also can be used to evaluate how close a mechanism tends to be singular. Singularities in parallel manipulators usually have been associated with either losing or gaining one or more DOF, cut a workspace apart into several pieces and hinder further applications, such as trajectory planning and control. So far, various approaches, most of which are based on Jacobian analysis, have been developed to address this problem. According to the previous work,[24,25] singularity for parallel mechanism can be generally classified into three main types: constraint singularity, inverse kinematic singularity, direct kinematic singularity.

(1) Constraint singularity

This kind of singularity depends on the alteration of the constraints acted on the platform within the workspace. Here the platform suffers from three force wrench constraints, which restrain spatial translations, provided by the constraint limb. In fact, constraint singularity happens for the four mechanisms if and only if the three axes of the serial spherical mechanism are coplanar, but the pose doesn't lie in the prescribed workspace.

(2) Inverse kinematic singularity

This kind of singularity occurs when $\det(\mathbf{J}_q) = 0$. For the ARDS1-N and ARDS2-N, $\mathbf{J}_q = \mathrm{diag}[1, 1, 1]$, the unit matrix will never degenerate, so the two mechanisms don't have this type singularity. For the ARDS1-R and ARDS2-R, $\boldsymbol{J}_q = \mathrm{diag}[1, 1, 1\ ({}^b\mathbf{b}_4 \times \mathbf{s}_4^r)^\tau\ {}^1\mathbf{s}_4]$, the diagonal matrix degenerates if and only if the following equation is tenable.

$$\left({}^b\mathbf{b}_4 \times \mathbf{s}_4^r\right)^\tau\ {}^1\mathbf{s}_4 = 0 \tag{19}$$

The above equality is satisfied as the ${}^1\boldsymbol{s}_4$ lies on the plane containing the vectors ${}^b\boldsymbol{b}_4$ and $\mathbf{s}_4^r$, that is, all the three axes of the serial spherical mechanism are coplanar and the constraint limb reaches its boundary. Hence, this type of singularity for the ARDS1-R and ARDS2-R lies out of the prescribed workspace, and simultaneously occurs with the constraint singularity.

(3) Direct kinematic singularity

This kind of singularity occurs when the matrix $\mathbf{J}_x$ or $\mathbf{J}_{xn}$ ($\mathbf{J}_x$ for the ARDS1-R and ARDS2-R, $\mathbf{J}_{xn}$ for the ARDS1-N and ARDS2-N) degenerates. As opposed to the second type, this one lies inside the workspace and should be carefully computed. According to Eq. (14), the square matrix $\mathbf{J}_{xn}$ consists of three vectors (${}^b\mathbf{b}_i \times \mathbf{s}_i^r$), and degenerates if $\det(\mathbf{J}_{xn}) = 0$ or $\mathrm{rank}(\mathbf{J}_{xn}) < 3$; the 4×3 non-square matrix $\mathbf{J}_x$ consists of four vectors, and the rank deficiency results from $\mathrm{rank}(\mathbf{J}_x) < 3$. However, it's tough to solve the equality $\det(\mathbf{J}_x) = 0$ or the inequality $\mathrm{rank}(\mathbf{J}_x) < 3$ in analytical expressions, so the possible method is to use numerical computation. Because $\mathbf{J}_{xn}$ is a square matrix, its condition number can be easily calculated by its eigenvalues. Although the matrix $\mathbf{J}_x$ is a non-square matrix, its condition number can be still accessed through using Eqs. (17) and (18). Hence, through computing the eigenvalues of the matrix $\mathbf{J}_x^T\mathbf{J}_x$ and the singular values of $\mathbf{J}_x$, it can be judged whether the matrix $\mathbf{J}_x$ degenerates. If the Jacobian matrix $\mathbf{J}_x$ degenerates, the minimum of singular values is zero and the condition number of $\mathbf{J}_x$ is infinity. As mentioned above, the higher the condition number is, the closer to singularity a mechanism is. Therefore, the condition number of $\mathbf{J}_x$ or $\mathbf{J}_{xn}$ can be used to evaluate how far away parallel manipulators are from singularity. Considering the aforementioned dexterity analysis results, the mechanism is deemed to be almost close to singularity when the matrix $\mathbf{J}_x$ or $\mathbf{J}_{xn}$ has a condition number greater than 1000. Through searching the region of interest in task space, platform orientations with condition numbers over the limit can be found. The fact is that there is no condition number beyond the designated limit for the matrix $\mathbf{J}_x$, that is, the ARDS1-R and ARDS2-R manipulators have no direct kinematic singularity within the prescribed workspace, but it's not true for the ARDS1-N and ARDS2-N, singular zones of which within the designated workspace are separately presented in Figs. 10(a) and 10(b). Figure 10(a) reveals that the points of the condition number more than 1000 nearly form a saddle surface spreading between the planes of $\gamma = -20$ deg and 20 deg that divides the workspace of the ARDS1-N into two parts; the singular surface of the ARDS2-N illustrated in Fig. 10(b) is a more twisted saddle surface, even spreading all over the workspace. These singular surfaces mean that the ARDS1-N and ARDS2-N manipulators can only continuously operate in one part per time, which is bad for ankle rehabilitation that needs

https://doi.org/10.1017/S0263574714000241 Published online by Cambridge University Press

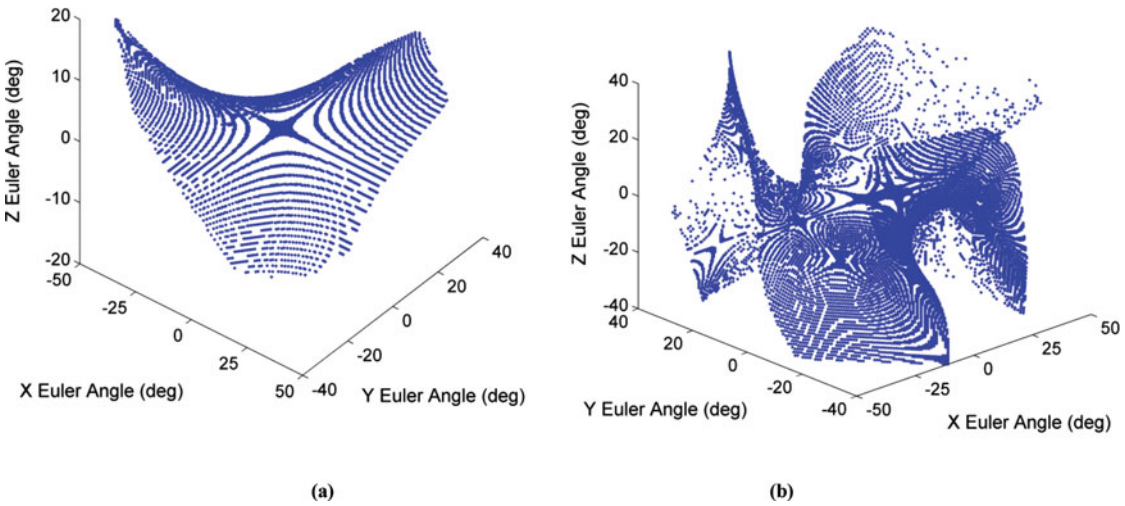

Fig. 10. Regions close to singularity with condition number >1000 for the ARDS1-N (a) and ARDS2-N (b).

full range motion. Meanwhile, it can be observed that the singularity zones depicted in Figs. 10(a) and 10(b) are in accordance with the regions with large condition number presented in Figs. 8(c) and 9(c) respectively.

Based on the distributions of singularity and dexterity, the ARDS1-R can easily switch between two modes depending on some control strategies: actuating the R_1 joint when close to singularity; free the R_1 joint when dexterity is much better in this mode. Similarly, the ARDS2-R also has another mode: by virtual of the partially decouple kinematical feature of the constraint limb, when the actuator of the R_1 joint is self-locked, the ARDS2-R can be reconfigured into a2-DOF 3-UPS/U mechanism, still redundantly actuated and performing plantar/dorsiflexion and inversion/eversion, which kinematical performance is also different from the aforementioned mechanisms as[23] researched. In conclusion, dexterity and singularity analyses prove the viewpoint that the actuator redundancy arrangement proposed in this paper can improve the dexterity value and eliminate singularity in the prescribed workspace.

4.4. Stiffness analysis

Stiffness is one of the most important performances of parallel mechanisms, because it reflects the amount of deflection as the moving platform suffers from external forces or moments. It's important for an ARD to have reasonable stiffness, since it needs certain stiffness to achieve the passive ROM exercise and keep patients safe simultaneously. Our objective is to explore the impact on stiffness resulting from actuator redundancy for further application. Many previous works[26,27] have established various kinds of stiffness models, involving several factors, such as the size and material of the links, mechanical transmission mechanisms, actuators, control system and even internal preload torque distribution for parallel mechanisms with actuator redundancy.[28] In this paper, actuators stiffness is considered as the main source of the stiffness of the four mechanisms. The following discussion on stiffness modeling will be based on this viewpoint.

Let $\mathbf{M} = [m_x, m_y, m_z]^T$ be the three-dimensional vector of end-effector output moment, $\boldsymbol{\Delta}\theta = [\Delta\theta_x, \Delta\theta_y, \Delta\theta_z]^T$ denote the vector of virtual angular displacement of the platform, $\boldsymbol{\tau} = [\tau_1, \tau_2, \tau_3, \tau_4]^T$ denote the vector of actuated joints forces, $\boldsymbol{\Delta}q = [\Delta q_1, \Delta q_2, \Delta q_3, \Delta q_4]^T$ denote the vector of virtual displacement associated with the active joints. Applying the principle of virtual work results in

$$\mathbf{w}^T\mathbf{M} = \dot{\mathbf{q}}^T\tau \tag{20}$$

Substituting Eq. (15) into Eq. (20) leads to

$$\mathbf{M} = \mathbf{J}^T\tau \tag{21}$$

https://doi.org/10.1017/S0263574714000241 Published online by Cambridge University Press

According to the definition of Jacobian matrix and Eq. (15), the following equation can be obtained:

$$\mathbf{J}\Delta\theta = \Delta\mathbf{q}. \tag{22}$$

Furthermore, τ can be associated with $\Delta\mathbf{q}$ using a 4×4 diagonal matrix $\chi = \text{diag}\,[k_1, ...k_i..., k_4]$ in which each diagonal element signifies the stiffness of the ith joint actuator. The relationship can be represented as follows:

$$\Delta\mathbf{q} = \chi^{-1}\tau. \tag{23}$$

Substituting Eqs. (23) and (22) into Eq. (21) leads to

$$\mathbf{M} = \mathbf{J}^T\chi\,\Delta\mathbf{q} = \mathbf{J}^T\chi\mathbf{J}\Delta\theta. \tag{24}$$

Hence, the stiffness matrix can be written as

$$\mathbf{K} = \mathbf{J}^T\chi\mathbf{J}. \tag{25}$$

It should be noted from Eq. (25) that the stiffness is mainly determined by the singular values or eigenvalues of the matrix $\mathbf{J}$ and changes with the variation of the manipulator configurations in workspace. There are many ways for stiffness evaluation, such as the determinant, the condition number, and the eigenvalues of the stiffness matrix.[27] Here the minimum and maximum eigenvalues are selected, for they reveal the limits of stiffness in the corresponding eigenvectors. For comparison among the four mechanisms, the stiffness constant for all prismatic actuators is set to 10^5 N/m, and for the revolute actuator is set to 10^5 Nm/rad too. The maximum and minimum eigenvalues of stiffness matrixes of the four mechanisms at each pose within the predefined workspace have been computed at various values of Euler angle γ. Figures 11 and 12 illustrate the distributions for the minimum and maximum eigenvalues in the plane of $\gamma = 0$ deg. Based on the results, the following inferences confirmed by other numerical computations in different γ values as well can be concluded.

(1) The maximum stiffness eigenvalues of the ARDS1-R and ARDS2-R are respectively rather higher than the ones of the ARDS1-N and ARDS2-N.
(2) The minimum stiffness eigenvalues of the ARDS1-R and ARDS2-R are respectively quite higher than the ones of the ARDS1-N and ARDS2-N.
(3) For the non-redundant ARDS1-N and ARDS2-N, the minimum stiffness close to a singular configuration is almost equal to zero; however, the redundant ARDS1-R and ARDS2-R still possess a sound stiffness index.
(4) For the redundant ARDS1-R and ARDS2-R, the minimum stiffness eigenvalues in the middle part of the workspace is always superior to ones around the boundary of the workspace; Fig. 11(b) shows the minimum stiffness eigenvalues of the ARDS1-R are almost around 800 in the middle workspace, and the minimum stiffness eigenvalues of the ARDS2-R are almost around 2000 shown in Fig. 12(b), so the ARDS2-R has better minimum eigenvalues than the ARDS1-R.

As discussed earlier, the eigenvalues of the stiffness matrix $\mathbf{K}$ are mainly dependent on the singular values of the Jacobian matrix $\mathbf{J}$, so the minimum eigenvalue of the matrix $\mathbf{K}$ inevitably tends to a small value when the condition number of the matrix $\mathbf{J}$ is very small. It is reasonable to say that the distribution of the condition number considerably reflects the trend of the minimum eigenvalues. Therefore, in view of Figs. 8(d) and 9(d), the conclusion can be testified again that the minimum eigenvalues of the ARDS1-R and ARDS2-R possess sound values in the middle of the workspace and smaller values at the boundary, and the minimum eigenvalues of the ARDS2-R is superior to the ones of the ARDS1-R. On all accounts, in terms of this analysis, the proposed actuator redundancy design can significantly improve the stiffness of parallel manipulators; the stiffness of the actuator of the R_1 joint has a great impact on the stiffness of the ARDS1-R and ARDS2-R, so it's critical for good performance to select a proper motor to actuate the R_1 joint.

https://doi.org/10.1017/S0263574714000241 Published online by Cambridge University Press

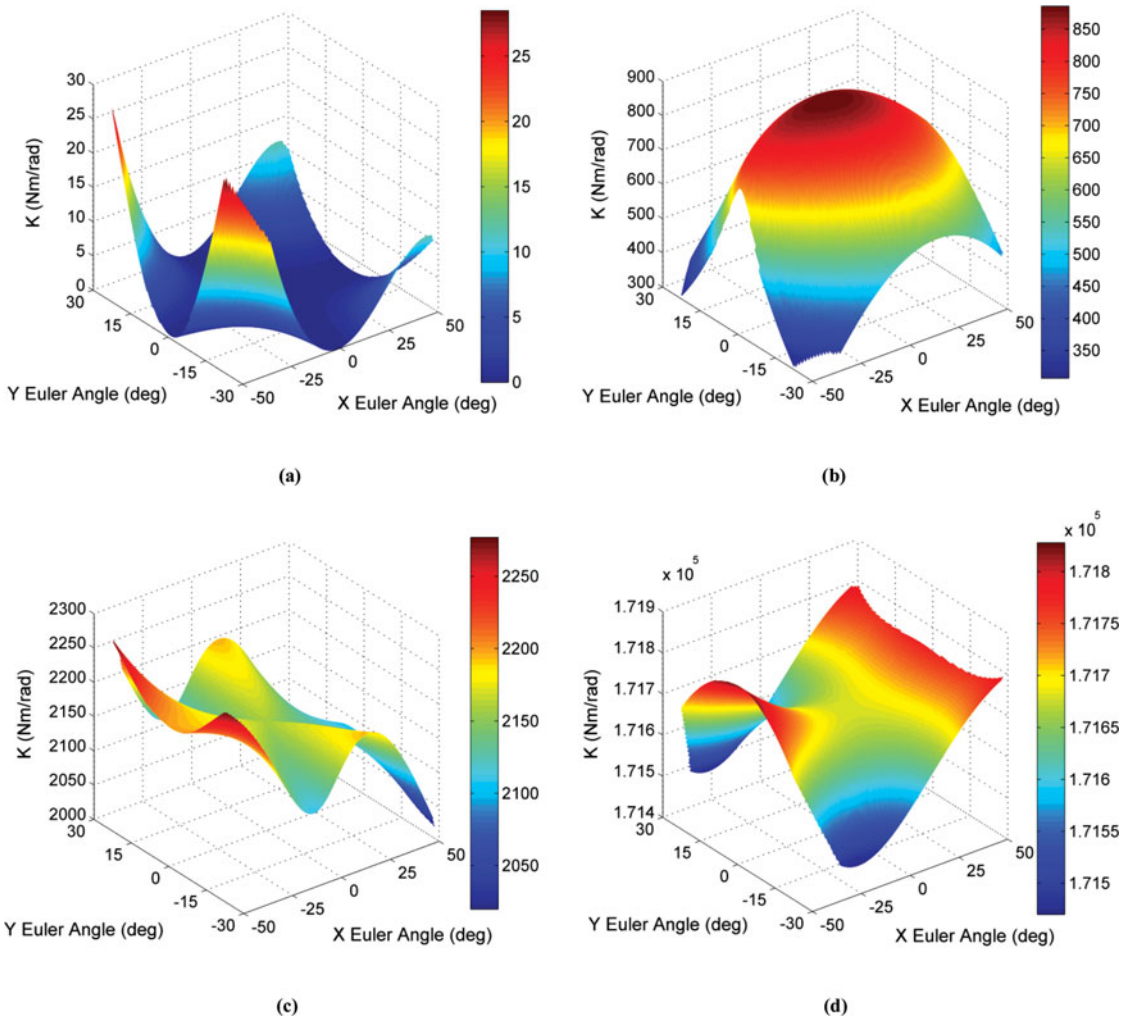

Fig. 11. The distribution of the minimum eigenvalues for the ARDS1-N (a) and ARDS1-R (b) in the plane of $\gamma = 0^\circ$; the distribution of the maximum eigenvalues for the ARDS1-N (c) and ARDS1-R (d) in the plane of $\gamma = 0^\circ$.

5. Conclusions and Future Work

The work reported in this paper shows that there exist at least two advantages for substituting a single spherical joint with two redesigned serial spherical mechanisms based on the conceptual design. One advantage is that we can easily fabricate several redundantly actuated parallel mechanisms for ankle rehabilitation, which are not only capable of actualizing the 3-DOF rotations, but also guarantee the mechanism center of rotation matches the ankle axes of rotation as closely as possible. Subsequently, the kinematical performance analyses show that the new arrangement of actuator redundancy can ensure the redundantly actuated ARDS1-R and ARDS2-R manipulators have no singularity, better dexterity and stiffness within the prescribed workspace in comparison with the corresponding non-redundantly actuated ARDS1-N and ARDS2-N manipulators. In fact, the ARDS2-R has much better dexterity and stiffness than the ARDS1-R, but the ARDS1-R can easily switch between two modes based on certain control strategies, actuating the R_1 joint when close to singularity and freeing the R_1 joint when dexterity is much better in this mode, to obtain better performance. Moreover, the ARDS2-R can be reconfigured into a 2-DOF 3-UPS/U mechanism when the actuator of the R_1 joint is self-locked. The second advantage is just the reconfigurable capacity possessed by the ARDS1-R and ARDS2-R. All the results show that the proposed serial spherical mechanisms have different kinematical characteristics, and the constructed parallel mechanisms based on them are suitable for ankle rehabilitation. Furthermore, how to optimize design parameters, customize actuators and build the real prototype will be discussed later.

https://doi.org/10.1017/S0263574714000241 Published online by Cambridge University Press

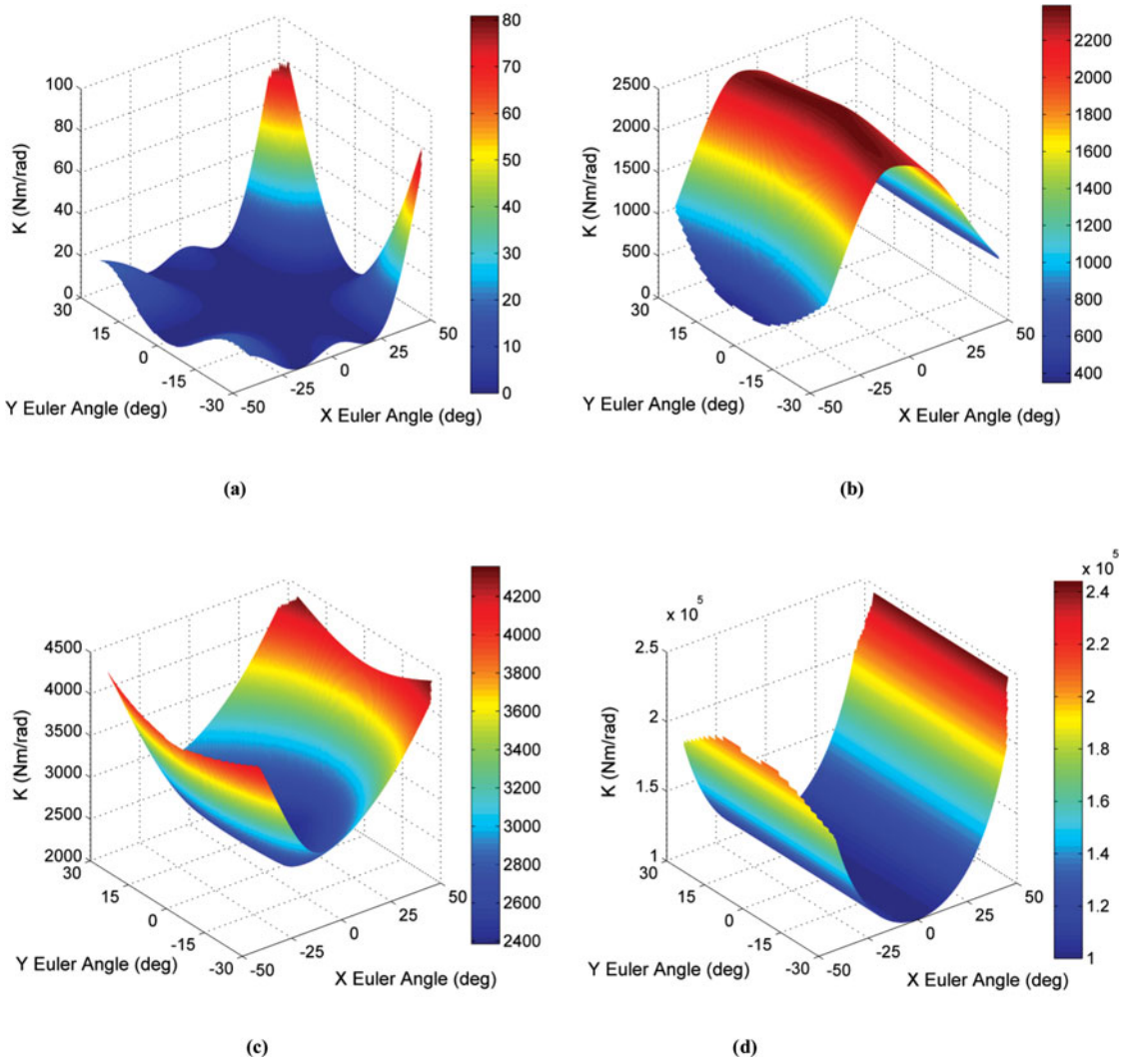

Fig. 12. The distribution of the minimum eigenvalues for the ARDS2-N (a) and ARDS2-R (b) in the plane of $\gamma = 0^\circ$; the distribution of the maximum eigenvalues for the ARDS2-N (c) and ARDS2-R (d) in the plane of $\gamma = 0^\circ$.

Acknowledgements

The authors gratefully acknowledge the financial support of National Science Foundation of China under grant No.51075025 and No.51175029, the Fundamental Research Funds for the Central Universities under grant No. 2012YJS101 and Beijing Natural Science Foundation (3132019). The authors also would like to express the deepest appreciation to the anonymous reviewers for the constructive comments.

References

1. I. Díaz, J. J. Gil and E. Sánchez, "Lower-limb robotic rehabilitation: literature review and challenges," *J. Robot.* **2011**, 1–11 (2011).
2. J. A. Blaya and H. Herr, "Adaptive control of a variable-impedance ankle-foot orthoses to assist drop-foot gait," *IEEE Trans. Neural Syst. Rehabil. Eng.* **12**(1), 24–31 (2004).
3. D. P. Ferris, K. E. Gordon, G. S. Sawicki and A. Peethambaran, "An improved powered ankle-foot orthosis using proportional myoelectric control," *Gait Posture* **23**, 425–428 (2006).
4. A. Roy, H. I. Krebs, D. J. Williams, C. T. Bever, L. W. Forrester, R. M. Macko and N. Hogan, "Robot-aided neurorehabilitation: A novel robot for ankle re-habilitation," *IEEE Trans. Rob.* **25**(3), 569–582 (2009).
5. S. Dong, K. Q. Lu, J. Q. Sun and K. Rudolph, "A prototype rehabilitation device with variable resistance and joint motion control," *Med. Eng. Phys.* **28**(4), 348–355 (2006).

https://doi.org/10.1017/S0263574714000241 Published online by Cambridge University Press

6. J. Yoon and J. Ryu, "A Novel Reconfigurable Ankle/Foot Rehabilitation Robot," *IEEE International Conference on Robotics and Automation*, Barcelona, (Apr. 2005) pp. 2290–2295.
7. Y. Ding, M. Sivak, B. Weinberg, C. Mavroidis and M. K. Holden, "NUVABAT: Northeastern University Virtual Ankle and Balance Trainer," *IEEE Haptics Symposium*, Waltham (Mar. 25–26, 2010) pp. 509– 514.
8. Biodex, Dynamometers (2013), http://www.biodex.com/physical-medicine/products/dynamometers/system-4-pro.
9. M. Girone, G. Burdea and M. Bouzit, "Rutgers ankle orthopedic rehabilitation interface," *Proc. ASMEDSC*, **67**, 305–312 (1999).
10. J. S. Dai and T. Zhao, "Sprained ankle physiotherapy based mechanism synthesis and stiffness analysis of a robotic rehabilitation device," *Auton. Robot* **16**(2), 207–218 (2004).
11. G. Liu, J. Gao, H. Yue, X. Zhang and G. Lu, "Design and Kinematics Analysis of Parallel Robots for Ankle Rehabilitation," *IEEE/RSJ International Conference on Intelligent Robots and Systems*, Beijing (Oct. 9–15, 2006) pp. 253–258.
12. J. A. Saglia, N. G. Tsagarakis, J. S. Dai and D. G. Caldwell, "A High Performance 2-Dof Over-Actuated Parallel Mechanism for Ankle Rehabilitation," *IEEE International Conference on Robotics and Automation*, Kobe (May 12–17, 2009) pp. 2180–2186.
13. Y. H. Tsoi and S. Q. Xie, "Design and control of a parallel robot for ankle rehabilitation," *Int. J. Intell. Syst. Technol. Appl.* **8**, 100–113 (2010).
14. Kidport, Ankle joint and bones, http://www.kidport.com/reflib/science/humanbody/skeletalsystem/Ankle.htm.
15. E. Sung, A. H. Slocum, R. Ma, J. F. Bean and M. L. Culpepper, "Design of an ankle rehabilitation device using compliant mechanisms," *J. Med. Device* **5**(1), 01101–7 (2011).
16. M. Dettwyler, A. Stacoff, I. A. Quervain and E. Stussi, "Modelling of ankle joint complex. Reflections with regards to ankle prostheses," *Foot Ankle Surg.* **10**(3), 109–119 (2004).
17. R. Clavel, "Device for the movement and positioning of an element in space," U.S. Patent, 4976582 (1990).
18. O. Company, F. Marquet and F. Pierrot, "A new high-speed 4-DOF parallel robot synthesis and modeling issues," *IEEE Trans. Robot. Autom.* **19**(3), 411–420 (2003).
19. B. Siciliano, "The Tricept robot: Inverse kinematics, manipulability analysis and closed-loop direct kinematics algorithm," *Robotica* **17**(4), 437–445 (1999).
20. C. M. Gosselin and J. Hamel, "The Agile Eye: A high –Performance Three-Degree-of-Freedom Camera-Orienting Device," *Proceedings of the IEEE International Conference on Robotics and Automation*, San Diego (1994) pp. 781–786.
21. J. Gallardo-Alvarado, A. Ramirez-Agundis, H. Rojas-Garduno and B. Arroyo-Ramirez, "Kinematics of an asymmetrical three-legged parallel manipulator by means of the screw theory," *Mech. Mach. Theory* **45**, 1013–1023 (2010).
22. J. P. Merlet, "Jacobian, manipulability, condition number, and accuracy of parallel robot," *ASME J. Mech. Des.* **128**(1), 199–206 (2006).
23. J. A. Saglia, J. S. Dai and D. G. Caldwell, "Geometry and kinematic analysis of a redundantly actuated parallel mechanism that eliminates singularities and improves dexterity," *ASME J. Mech. Des.* **130**(12), 124501–5 (2008).
24. C. M. Gosselin and J. Angeles, "Singularity analysis of closed-loop kinematic chains," *IEEE Trans. Robot. Autom.* **6**(3), 281–290 (1990).
25. Y. F. Fang and L. W. Tsai, "Structure synthesis of a class of 4-DOF and 5-DOF parallel manipulators with identical limb structures," *Int. J. Rob. Res.* **21**(9), 799–810 (2002).
26. S. Joshi and L. W. Tsai, "A comparison study of two 3-DOF parallel manipulators: One with three and the other with four supporting limbs," *IEEE Trans. Robot. Autom.* **19**, 200–209 (2003).
27. Y. Li and Q. Xu, "Stiffness analysis for a 3-PUU parallel kinematic machine," *Mech. Mach. Theory* **43**, 186–200 (2008).
28. H. Shin, S. Lee, J. I. Jeong and J. Kim, "Antagonistic stiffness optimization of redundantly actuated parallel manipulators in a predefined workspace," *IEEE/ASME Trans. Mechatronics* **18**(3), 1161–1169 (2013).